CHEMISTRY
A EUROPEAN JOURNAL

DOI: 10.1002/chem.201000153

Phenakite-Type BeP_2N_4—A Possible Precursor for a New Hard Spinel-Type Material

Florian J. Pucher, S. Rebecca Römer, Friedrich W. Karau, and Wolfgang Schnick*[a]

Abstract: BeP_2N_4 was synthesized in a multi-anvil apparatus starting from Be_3N_2 and P_3N_5 at 5 GPa and 1500 °C. The compound crystallizes in the phenakite structure type (space group $R\bar{3}$, no. 148) with $a = 1269.45(2)$ pm, $c = 834.86(2)$ pm, $V = 1165.13(4) \times 10^6$ pm^3 and $Z = 18$. As isostructural and isovalence-electronic α-Si_3N_4 transforms into β-Si_3N_4 at high pressure and temperature, we studied the phase transition of BeP_2N_4 into the spinel structure type by using density functional theory calculations. The predicted transition pressure of 24 GPa is within the reach of today's state of the art high-pressure experimental setups. Calculations of inverse spinel-type BeP_2N_4 revealed this polymorph to be always higher in enthalpy than either phenakite-type or spinel-type BeP_2N_4. The predicted bulk modulus of spinel-type BeP_2N_4 is in the range of corundum and γ-Si_3N_4 and about 40 GPa higher than that of phenakite-type BeP_2N_4. This finding implies an increase in hardness in analogy to that occurring for the β- to γ-Si_3N_4 transition. In hypothetical spinel-type BeP_2N_4 the coordination number of phosphorus is increased from 4 to 6. So far only coordination numbers up to 5 have been experimentally realized (γ-P_3N_5), though a sixfold coordination for P has been predicted for hypothetic δ-P_3N_5. We believe, our findings provide a strong incentive for further high-pressure experiments in the quest for novel hard materials with yet unprecedented structural motives.

Keywords: density functional calculations · high-pressure chemistry · nitridophosphate · phase transitions · spinel phases

Introduction

Phosphorus(V) nitride P_3N_5 has long been known as a refractory binary nitride and has been used in a multitude of applications, for example, as a gate insulator material in metal-insulator semiconductor field-effect transistors (MISEETs),[1–3] as a getter material in incandescent and tungsten-halogen lamps,[4] or as a flame retardant.[5] The compound has been known for quite a long time,[6] even though its structure was not solved until 1997.[7] Similar to other nonmetal nitrides (e.g., Si_3N_4), P_3N_5 is built up solely by TN_4 tetrahedra (T = P, Si, …) forming a three-dimensional network structure. Yet it exhibits not only corner sharing, but also edge sharing tetrahedra, which are a unique building block for binary nitrides. A significant increase in density and mechanical hardness is achieved upon transformation into the high-pressure polymorph γ-P_3N_5.[8,9] In accordance to the pressure-coordination rule, a partial increase of the coordination number of phosphorus from 4 to 5 occurs, thus leading to a coordination according to $P^{[4]}P_2^{[5]}N^{[2]}N_4^{[3]}$. At higher pressures (about 40 GPa) theoretical studies suggest a transformation into hypothetic δ-P_3N_5 with a kyanite-type structure comprising PN_6 octahedra and PN_4 tetrahedra.[10] δ-P_3N_5 may well distort upon quenching to ambient conditions along a shear distortion path, resulting in monoclinic δ'-P_3N_5 built up of PN_6 octahedra, PN_5 trigonal bipyramids, and PN_4 tetrahedra.[10]

During the last few years, we succeeded in the high-pressure/high-temperature syntheses of a number of multinary nitridophosphates starting from P_3N_5 and the respective azides. Azides have proven to be very successful precursors, as they decompose into the corresponding nitrides and nitrogen under high-pressure/high-temperature conditions, which then react with P_3N_5 to give the desired product.[11] The nitrogen released from the azides helps to prevent a thermal dissociation of the target compound. Furthermore, the use of azides circumvents the problem of non-existing or difficult to synthesize nitrides (e.g., Na_3N and K_3N). Employing the so-called azide-route, recently we were able to

[a] F. J. Pucher, Dr. S. R. Römer, Dr. F. W. Karau, Prof. Dr. W. Schnick
Department Chemie
Lehrstuhl für Anorganische Festkörperchemie
Ludwig-Maximilians-Universität
Butenandtstrasse 5–13, 81377 München (Germany)
Fax: (+49) 89-2180-77440
E-mail: wolfgang.schnick@uni-muenchen.de

Supporting information for this article is available on the WWW under http://dx.doi.org/10.1002/chem.201000153.

synthesize a variety of new nitridophosphates, among them the first nitridic clathrate $P_4N_4(NH)_4(NH_3)$,[12] MP_4N_7 (M^I = Na–Cs)[13] and MP_2N_4 (M^{II} = Ca, Sr, Ba).[14–16]

Within our systematic investigation of group II nitridophosphates we now succeeded in the synthesis of BeP_2N, which crystallizes in the phenakite structure type. As BeP_2N_4 is isotypic and isoelectronic to β-Si_3N_4, which can transform into spinel-type γ-Si_3N_4 at 15 GPa,[17,18] a high-pressure phase transition into spinel-type BeP_2N_4 is considered and assessed by density functional theory (DFT) calculations. γ-Si_3N_4 has been found to be a very hard material.[19] Spinel-type BeP_2N_4 may well show similar mechanical properties, as phenakite-type BeP_2N_4 is already hard enough to scratch agate (Mohs Hardness: 6.5–7).[20]

Results and Discussion

Synthesis of BeP_2N_4: BeP_2N_4 was synthesized from Be_3N_2 and P_3N_5 in a multi-anvil press at 5 GPa and 1500 °C according to Equation (1).

$$Be_3N_2 + 2\,P_3N_5 \rightarrow 3\,BeP_2N_4 \qquad (1)$$

To improve crystallinity and remove phosphorus impurities, the reaction product was annealed for 2 h in a nitrogen atmosphere at 680 °C. For further details on the synthesis, see the Experimental Section.

Structure determination of BeP_2N_4: The crystal structure of BeP_2N_4 was determined from X-ray powder diffraction data obtained by using a Stoe StadiP diffractometer in Debye–Scherrer geometry using $Cu_{K\alpha1}$ radiation. The diffraction pattern was indexed using the WERNER-algorithm, as implemented in WinXPOW.[21–24] The structure was found to be rhombohedral primitive with lattice parameters a = 1269.45(2) pm and c = 834.86(2) pm (hexagonal setting). As a starting model for the Rietveld refinement a modified structure model of phenakite Be_2SiO_4 was employed. All Be positions of phenakite were occupied by P, Si positions by Be and O positions by N. Impurities (phosphorus or hexagonal and cubic Be_3N_2) were fitted using the Le Bail method and subtracted internally by the program from the diffraction pattern during the refinement. Structure refinement was possible both for the raw product as well as for annealed samples. However, better results were obtained from powder diffraction data of annealed samples due to improved crystallinity. All data given here refer to annealed BeP_2N_4. For details on the structure refinement, see Experimental Section.

The atomic positions and isotropic thermal displacement factors of BeP_2N_4 are given in Table 1, the crystallographic data in Table 2.

Structure description of BeP_2N_4: BeP_2N_4 crystallizes in the trigonal space group $R\bar{3}$ no. 148), isotypic with phenakite Be_2SiO_4.[25] The structure is built up of all corner sharing BeN_4 and PN_4 tetrahedra, resulting in a coordination description according to $Be^{[4]}P_2^{[4]}N_4^{[3]}$. The tetrahedra form dreier, vierer and sechser rings,[26] the latter two forming channels parallel to [001] (Figure 1), while the dreier rings

Table 1. Atom positions and isotropic displacement factors of BeP_2N_4.

Atom	x	y	z	U_{iso}
Be(1)	0.2080(20)	0.2223(20)	0.249(4)	0.25
P(1)	0.2127(5)	0.0208(4)	0.4165(7)	2.24(17)
P(2)	0.2011(5)	0.0061(5)	0.0770(7)	4.14(20)
N(1)	0.1936(10)	0.0730(8)	0.2486(15)	0.29(11)
N(2)	0.3318(11)	0.3297(11)	0.2611(16)	0.29(11)
N(3)	0.1293(10)	0.2158(10)	0.0805(15)	0.29(11)
N(4)	0.1297(13)	0.2275(10)	0.4192(15)	0.29(11)

Table 2. Crystallographic data of BeP_2N_4.

	BeP_2N_4
M_w [g mol^{-1}]	126.99
crystal system	trigonal
space group	$R\bar{3}$ (No. 148)
a [pm]	1268.97(2)
c [pm]	834.69(2)
V [10^6 pm^3]	1164.01(4)
formula units percell	18
ρ [g cm^{-3}]	3.258
diffractometer	Stoe StadiP
radiation	$CuK_{\alpha1}$ (λ = 154.056 pm)
detector	lin. PSD $\Delta 2\theta$ = 5°
step width [°]	0.03
internal step width [°]	0.01
2θ-range [°]	$10.0 \le 2\theta \le 80.0$
data points	6785
obs. Reflections	163
background function	shifted Chebyshev
no. of coefficients	18
profile function	pseudo-Voigt
R_p	0.0864
wR_p	0.1161
R_{pBknd}	0.0971
wR_{pBknd}	0.1264
$R_{\|F\|}2$	0.1290

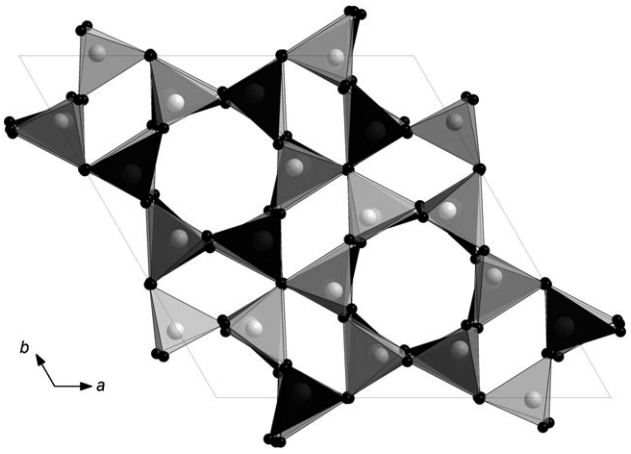

Figure 1. Crystal structure of phenakite-type BeP_2N_4 (view along [001]; BeN_4 tetrahedra depicted black, PN_4 tetrahedra depicted gray.

exist only orthogonal to [001] (see the Supporting Information). Two thirds of the sechser rings in each unit cell are built up by alternating BeN_4 and PN_4 tetrahedra, one third only by PN_4 tetrahedra (cf. Figure 1).

All N atoms are coordinated by one Be and two P atoms, resulting in almost regular trigonal planar coordination. The three T-N-T angles sum up to values between 355.5° and 359.3°, which differ only slightly from the regular value of 360° for planarity. The angles N-T-N within the TN_4 tetrahedra range from 98.7(7) to 118.6(6)° (PN_4) and from 101.4(15) to 117.9(15)° (BeN_4) and thus are close to the regular tetrahedron angle of 109.5° (Table 3 and the Supporting Information). The bond lengths Be–N are found to be 148.1(19)–181.1(23) pm, while the P–N bond lengths vary from 160.3(10) to 173.0(13) pm (Table 4 and the Supporting Information), the latter matching perfectly values found in the literature for P–N (e.g., NaP_4N_7: 155.3–175.5 pm,[13] α-P_3N_5: 150.7–174.5 pm).[7]

Table 3. Tetrahedra angles and cation-anion-cation angles in BeP_2N_4 (experimental and calculated) as well as in phenakite[27] and β-Si_3N_4[28] (all angles given in°).

	N-P-N (O-Be-O)	N-Be-N (O-Si-O)	A-X-B (A,B=Be, P, Si; X=N, O)
BeP_2N_4	98.7(7)–118.5(6)	101.4(15)–117.9(15)	110.7(11)–125.9(13)
BeP_2N_4 (LDA)	108.70–112.50	107.11–109.38	110.48–127.98
BeP_2N_4 (GGA)	107.22–112.78	106.72–109.26	112.28–128.15
Be_2SiO_4	107.56–114.29	107.80–113.01	113.08–123.69
β-Si_3N_4	108.69–115.64	–	115.64–121.91

Table 4. Bond lengths in BeP_2N_4 (experimental and calculated), compared to values in α-P_3N_5[7] and α-Be_3N_2[29] (all bond lengths given in pm).

	$Be^{[4]}$–N	$P^{[4]}$–N
BeP_2N_4	148.1(19)–181.1(23)	160.3(10)–173.0(13)
BeP_2N_4 (LDA)	170.52–173.10	161.86–163.73
BeP_2N_4 (GGA)	172.58–175.99	163.58–165.47
α-P_3N_5 (*Cc*)	–	150.72–174.46
α-P_3N_5 (*C*2/*c*)	–	153.66–172.59
α-Be_3N_2	172.45–181.55	–
Σ ionic radii (Shannon)[30]	171	163
Σ ionic radii (Baur)[31]	175	158

DFT calculations: The structure optimization of BeP_2N_4 revealed a more ideal structure than experimentally found. This becomes clear when examining the *x* and *y* fractional coordinates of atoms placed above each other viewed along [001]. In β-Si_3N_4 they are identical, owing to the higher symmetry, and in phenakite, they are almost identical with only very small deviations. In BeP_2N_4 larger deviations are found (see the Supporting Information). A similar tendency is reflected in the tetrahedra angles N-P-N and N-Be-N compared to those in phenakite (O-Be-O and O-Si-O) and β-Si_3N_4 (N-Si-N) (Table 3). Again the values obtained from the optimized structures are closer to those found in phenakite and β-Si_3N_4 (Table 3).

The calculated bond lengths P–N and Be–N in comparison to the experimental values are given in Table 4. The spread of the calculated bond lengths is smaller than that for the experimentally determined structure. However, all values (with the exception of the Be–N bonds in BeP_2N_4) are similar to those found in α-P_3N_5[7] and α-Be_3N_2.[29] As for the very short value of 148.1(19) pm found experimentally for the Be–N bond length in BeP_2N_4, it seems clear that the calculated values are more reasonable.

BeP_2N_4 exhibits the phenakite structure like β-Si_3N_4,[28] which transforms into a spinel-type structure at high pressure (γ-Si_3N_4).[17,18] Si_3N_4 and BeP_2N_4 are iso-valence-electronic (32 valence electrons per formula unit) and the ionic radii of Be^{2+} (27 pm) and P^{5+} (17 pm) are comparable to those of Si^{4+} (26 pm).[30] Therefore, a spinel-type high-pressure phase of BeP_2N_4 seems to be likely.

Spinels are compounds of composition AB_2X_4. The anions X form a cubic close packing (ccp) and the cations occupy an eighth of the tetrahedral voids and half of the octahedral voids. In the normal spinel structure the A atoms occupy the tetrahedral voids, whereas the B atoms are located in the octahedral voids. In inverse spinels, half of the B atoms occupy tetrahedral sites and half occupy octahedral sites, whereas the A atoms occupy the remaining octahedral sites. In between these two types of spinel structures countless partly inverse spinel structures can be envisaged.[32]

We calculated BeP_2N_4 both in the normal as well as the inverse spinel structure. Normal spinel crystallizes in cubic space group $Fd\bar{3}m$ (no. 227). The Be atoms are located on the tetrahedral sites, the P atoms on the octahedral sites. Therefore, in normal spinel-type BeP_2N_4 (sp-BeP_2N_4), compared to phenakite-type BeP_2N_4, the coordination number of P would be increased from four to six for all P atoms. So far in nitridophosphates only coordination numbers of phosphorus up to five have been experimentally realized (cf. γ-P_3N_5)[8,9] and a sixfold coordination for P has been predicted for hypothetic δ-P_3N_5.[10]

To construct the inverse spinel structure, the primitive unit cell of normal spinel was used as a starting point. This cell contains two formula units, resulting in two tetrahedrally and four octahedrally coordinated cation positions. The tetrahedrally coordinated positions were solely occupied by P. For the distribution of the remaining P and Be atoms on the octahedral positions, from a combinatorial point of view, six patterns were possible. However, owing to symmetry reasons, all combinations resulted in the same structure (Figure 2). The resulting inverse spinel structure exhibits the orthorhombic space group *Imma* (no. 74) (see the Supporting Information). An inverse spinel high-pressure phase of BeP_2N_4 would result in a partially increased coordination number for P, as only half of the P atoms are occupying octahedral sites, whereas the coordination number for all Be would be increased from four to six, which, to the best

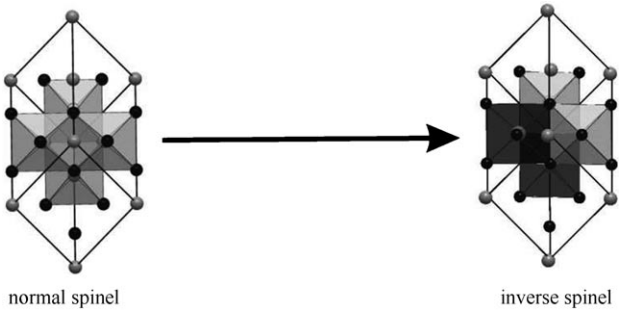

Figure 2. Construction of inverse spinel from the normal spinel structure (Be atoms drawn light gray, P atoms dark gray, N atoms black; Be/PN_6 octahedra are drawn, PN_6 octahedra light gray, BeN_6 octahedra black).

knowledge of the authors, is not yet known except for central Be in Zr_6 clusters.[33]

The calculated bond lengths for P–N and Be–N in spinel-type BeP_2N_4 and inverse spinel-type BeP_2N_4 are listed in Table 5. They are all in the range found in Be_3N_2 and P_3N_5 compounds.[7–9,29] $Be^{[6]}$–N distances are longer than $Be^{[4]}$–N distances, as are the bond lengths of $P^{[6]}$–N in comparison to the bond lengths of $P^{[4]}$–N.

Table 5. Bond lengths in normal (sp-) and inverse spinel-type (isp-)-BeP_2N_4, compared to values in γ-P_3N_5[8,9] and α-Be_3N_2[29] as well as the theoretically predicted P_3N_5 phases δ-P_3N_5[10] and δ′-P_3N_5[10] (all bond lengths given in pm).

	$Be^{[4]}$–N	$Be^{[6]}$–N	$P^{[4]}$–N	$P^{[5]}$–N	$P^{[6]}$–N
sp-BeP_2N_4 (LDA)	173.76	–	–	–	176.19
sp-BeP_2N_4 (GGA)	179.91	–	–	–	182.24
isp-BeP_2N_4 (LDA)	–	181.49	162.37	–	176.72
		184.53	172.23		181.39
isp-BeP_2N_4 (GGA)	–	183.39	164.05	–	178.93
		187.22	175.36		183.99
γ-P_3N_5	–	–	158.65	165.71–	–
			169.76	177.54	
δ-P_3N_5	–	–	156.3–	–	164.9–
			159.9		186.9
δ′-P_3N_5	–	–	153.9–	159.2–	174.3–
			165.7	187.1	185.1
α-Be_3N_2	172.45–	–	–	–	–
	181.55				

Phenakite-type BeP_2N_4 exhibits both, within LDA and GGA, the lowest ground state energy (LDA: −58.817 eV; GGA: −52.840 eV) and density. The calculated density (LDA: 3.31 $g\,cm^{-3}$; GGA: 3.20 $g\,cm^{-3}$) matches quite well the experimental value (3.26 $g\,cm^{-3}$). Spinel-type BeP_2N_4 is about 22% denser than phenakite-type BeP_2N_4 and 1.105 eV (LDA) and 1.611 eV (GGA), respectively, higher in energy. Inverse spinel-type BeP_2N_4 is the densest phase of the three considered (about 24–25% denser than phenakite-type BeP_2N_4 and about 2% denser than spinel-type BeP_2N_4). It leads to values 2.428 eV (LDA) and 2.979 eV (GGA) higher in energy than phenakite-type BeP_2N_4 and 1.323 eV (LDA) and 1.368 eV (GGA) higher than spinel-type BeP_2N_4.

Phenakite-type BeP_2N_4 exhibits the lowest bulk modulus (GGA: 220 GPa). Spinel-type BeP_2N_4 has a zero-pressure bulk modulus of 291 GPa within LDA and of 263 GPa within GGA. The highest bulk modulus was found for inverse spinel-type BeP_2N_4, which amounts to 316 GPa within LDA and to 278 GPa within GGA. All calculated values are listed in Table 6. A high bulk modulus is an indicator for

Table 6. E_0, V_0, B_0, and ρ_0 of phenakite-type, spinel-type (sp-) and inverse spinel-type (isp-)BeP_2N_4 within LDA and GGA (E_0 and V_0 given per formula unit).

	E_0 [eV]	V_0 [10^6 pm^3]	B_0 [GPa]	ρ_0 [$g\,cm^{-1}$]
BeP_2N_4 (LDA)	−58.817	63.66	–	3.31
sp-BeP_2N_4	−57.721	52.01	291	4.05
isp-BeP_2N_4	−56.389	50.97	316	4.14
BeP_2N_4 (GGA)	−52.840	65.99	220	3.20
sp-BeP_2N_4	−51.229	54.11	263	3.90
isp-BeP_2N_4	−49.861	53.11	278	3.97

hardness, but not in itself a sufficient precondition for it, as the hardness of a material is determined by various factors. It is widely accepted, that small atoms, short bonds, a high degree of covalency, a high bond density and a high packing efficiency are required for hard materials.[34,35] An increase of the coordination number on its own will not necessarily effect a higher hardness, as it not only increases the packing efficiency, but also bond length and ionicity. This results in opposed effects on the hardness and it remains to be seen which factor is dominant.[35] For spinel-type γ-Si_3N_4 an increase in hardness, as compared to β-Si_3N_4, is paralleled by an increase in bulk modulus. As BeP_2N_4 is isovalence-electronic to Si_3N_4, the ionic radii for Be^{2+} and P^{5+} are similar to that of Si^{4+}.[30,31] The phase transformation from phenakite-type to spinel-type BeP_2N_4 is also accompanied by an increase of the bulk modulus, and the bulk modulus of spinel-type BeP_2N_4 adopts a value between that of corundum (B_0=252 GPa, H_V=20 GPa)[36] and γ-Si_3N_4 (B_0 experimental=290–317 GPa,[37,38] B_0 calculated 292–319 GPa,[39] H_V=30–43 GPa),[37] spinel-type BeP_2N_4 is likely to exhibit a hardness similar to these compounds and higher than that of phenakite-type BeP_2N_4, which would render it a quite-hard material. Furthermore, its bulk modulus is comparable to those of other nitridic spinels (hypothetic *c*-Fe_3N_4: B_0= 304 GPa;[40] γ-Ge_3N_4: B_0=295 GPa[41]) and higher than the bulk modulus estimated for the mixed oxynitride Ga_3O_3N (B_0=234 GPa).[42]

Energy-volume calculations of high-pressure phase transitions: In Figure 3 the energy–volume curves calculated within GGA are depicted. From these, the enthalpy-pressure phase diagram, as depicted in Figure 4 was derived. Accordingly, the transition pressure of phenakite-type BeP_2N_4 into spinel-type BeP_2N_4 was calculated to 24 GPa within GGA. Inverse spinel-type BeP_2N_4 was found to be always higher in enthalpy than either phenakite-type or spinel-type BeP_2N_4 up to 100 GPa (also Figure 4). Therefore, only

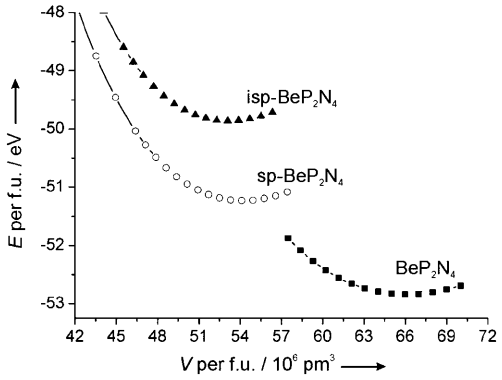

Figure 3. Energy-volume (E–V) phase diagram of phenakite-type, spinel-type (sp-) and inverse spinel-type (isp-)BeP_2N_4 (GGA; each symbol represents a calculation): isp-BeP_2N_4 (▲); sp-BeP_2N_4 (○); BeP_2N_4 (■).

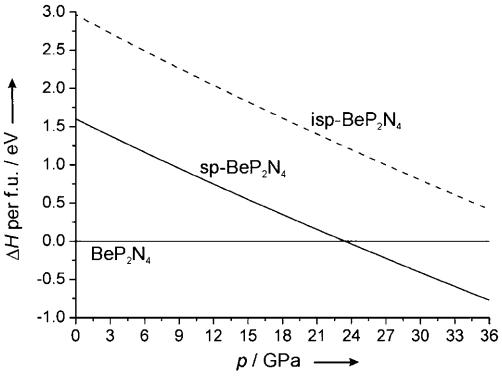

Figure 4. Enthalpy-pressure (H–p) diagram for the transition of phenakite-type BeP_2N_4 into spinel-type (sp-)BeP_2N_4 ($p_t = 24$ GPa). Inverse spinel-type (isp-)BeP_2N_4 remains always higher in enthalpy than either other polymorph (GGA, derived from the evaluation of the E–V data by the Murnaghan EOS).

spinel-type BeP_2N_4 seems to be a candidate for a high-pressure phase of BeP_2N_4.

The calculated transition pressure for phenakite-type BeP_2N_4 into spinel-type BeP_2N_4 is quite low, 24 GPa. This pressure is just out of reach of our multi-anvil setup but should be easily attainable in diamond anvil cell setups, even if, as a result of kinetic effects, the experimental transition pressure is somewhat higher than the calculated value.

Conclusion

BeP_2N_4, synthesized in a multi-anvil apparatus at 5 GPa and 1500 °C crystallizes in the phenakite structure. Higher crystallinity can be achieved by annealing the sample at 680 °C. Annealing also removes the by-product of black phosphorus, but leads to the formation of minor quantities of hexagonal and cubic Be_3N_2. The crystal structure was refined from powder diffraction data by using the Rietveld method.

Density functional calculations suggest a phase transformation into spinel-type BeP_2N_4 at about 24 GPa. This pressure range is well attainable in today's high-pressure experimental setups. The calculated bulk moduli for spinel-type BeP_2N_4, which are in the range of known hard materials, such as corundum and γ-Si_3N_4, are higher than that of phenakite-type BeP_2N_4, which proved hard enough to scratch agate.

Experimental Section

Synthesis of BeP_2N_4: BeP_2N_4 was synthesized from the binary nitrides Be_3N_2 and P_3N_5 at 1500 °C and 5 GPa by using a Walker-type multianvil apparatus. Be_3N_2 was synthesized from beryllium powder (Chempur) by heating to 1100 °C in a continuous flow of nitrogen.[43] P_3N_5 was obtained by heating hexachlorocyclotriphosphazene $(PNCl_2)_3$ (Aldrich, 99 %) in a continuous flow of ammonia (3.8, Messer Griesheim) and subsequent removal of ammonium chloride in vacuo.[44] Owing to the hydrolysis sensitivity of Be_3N_2, sample preparations were carried out in a glove box (MBraun MB 150, Garching, Germany; $H_2O \leq 0.2$ ppm, $O_2 \leq 1.0$ ppm) in an argon atmosphere. The starting materials phosphorus(V) nitride and beryllium nitride with a molar ratio of 2:1 were thoroughly mixed and ground in a micro-ball mill. The mixture was then packed into a hexagonal boron nitride crucible (Henze, Kempten, Germany) which afterwards was placed in the high-pressure experiment assembly. The crucible was centered within a set of two graphite resistance heaters and held in place using two spacers of MgO. This heating unit was thermally isolated from the outer assembly parts by a tube of ZrO_2, which was placed in a previously drilled hole in an octahedral pressure medium (Cr_2O_3 doped MgO, Ceramic Substrates). Electrical contact to the anvils of tungsten carbide was achieved by using two pieces of molybdenum. Owing to the toxicity of beryllium and its compounds,[45] the module was sealed prior to the experiment with silicone. The sample was compressed to 5 GPa within 4.5 h, then heated to 1500 °C within 40 min. The temperature was held for 30 min and then reduced to room temperature within 30 min, followed by a decompression period of 10 h. After the experiment the crucible was recovered and wetted with PTFE spray prior to breaking it open to obtain the reaction product. The raw product appeared to be black, due to impurities of black phosphorus and was hard enough to scratch agate. To remove the phosphorus from the sample, the raw product was sealed in a glass ampoule under nitrogen atmosphere, heated to 680 °C within 2 h, held at this temperature for 1 h and slowly cooled to room temperature. Black phosphorus is thus converted to white phosphorus, which evaporates and condenses onto the glass walls during cooling. The obtained BeP_2N_4 powder still contains minor traces of hexagonal and cubic Be_3N_2. To synthesize purer samples of BeP_2N_4, containing less phosphorus impurities, higher pressures of 8–12 GPa are of advantage.

Powder X-ray diffraction: X-ray diffraction experiments on powder samples of BeP_2N_4 were performed by using a STOE StadiP powder diffractometer in Debye–Scherrer geometry, with Ge(111)-monochromatized $Cu_{K\alpha 1}$ radiation ($\lambda = 154.06$ pm). Indexing the diffraction pattern using the WERNER-algorithm as implemented in WinXPOW[21–24] resulted in a rhombohedral primitive cell with lattice parameters $a = 1269.45(2)$ pm, $c = 834.86(2)$ pm (hexagonal setting). A Rietveld refinement has been carried out using the program package GSAS.[46] As a starting model for the Rietveld refinement a modified structure model of phenakite was used. The Be positions of phenakite were occupied by P, the Si positions by Be and the O positions by N. All not annealed samples of BeP_2N_4 contain traces of orthorhombic phosphorus. Its reflections were fitted using the Le Bail method and subtracted internally by the program from the powder diffraction pattern during the refinement. Diffraction patterns of annealed samples showed reflections that were assigned to hexagonal and cubic beryllium nitride. These were also fitted using the Le Bail method and subtracted internally by the program from the diffraction pattern during the refinement. The atomic positions of all atoms as well as the isotropic displacement factors of phosphorus were refined. Owing to the low scattering factor of Be, its thermal displacement factors could not be refined. The isotropic displacement factors of the N atoms

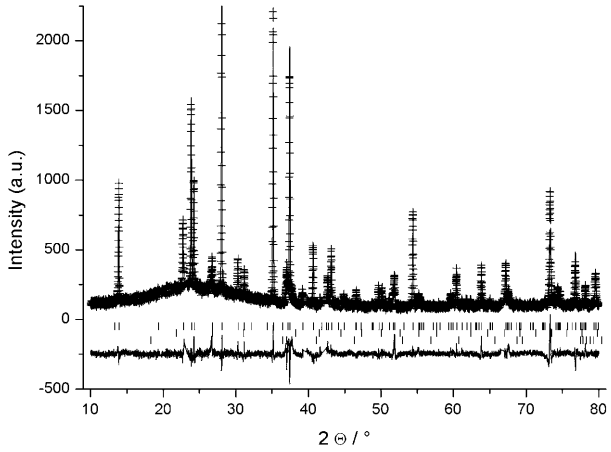

Figure 5. Rietveld refinement of BeP_2N_4, showing I_{obs} (crosses), I_{cal} (line), $I_{obs}-I_{cal}$. Allowed reflections of BeP_2N_4 as well as those of the by-products (hexagonal and cubic Be_3N_2) are marked with vertical lines.

were set to equal values and refined together. The observed and calculated X-ray powder diffraction pattern and the difference profile of the Rietveld refinement are shown in Figure 5.

Further details of the crystal structure investigations can be obtained from the Fachinformationszentrum Karlsruhe, 76344 Eggenstein-Leopoldshafen, Germany (fax: (+49)7247-808-666; e-mail: crysdata@fiz-karlsruhe.de) on quoting the depository number CSD-421385.

Computational methods: Structural optimizations, total energies, and properties are calculated within density functional theory (DFT),[47] for which we use the Vienna ab-initio Simulation Package (VASP). It combines the total energy pseudopotential method with a plane-wave basis set.[48–50] The electron exchange and correlation energy were treated within the local-density approximation (LDA)[51] as well as generalized-gradient approximation (GGA).[52,53] We employ the projector-augmented wave (PAW) method.[54,55] The cut-off energy for the expansion of the wave function into the plane wave basis was 500 eV. Residual forces were converged below 5×10^3 eV Å^{-1}. The Brillouin zone integration was done by using the Monkhorst-Pack scheme.[56] Structure optimizations were done by relaxing all internal parameters as well as cell parameters and the unit cell volume. The unit cell of BeP_2N_4 contains 126 atoms, which is reduced to 42 atoms (6 formula units) by employing the primitive unit cell. A k-point mesh of $6\times6\times6$ was used. The unit cell of spinel BeP_2N_4 contains 56 atoms. By transforming into a primitive unit cell, this is reduced to 14 atoms per cell (2 formula units). A *k*-point mesh of $6\times6\times6$ was used. The unit cell of inverse spinel BeP_2N_4 contains 28 atoms, the primitive cell 14 atoms (2 formula units). A k-point mesh of $6\times6\times6$ was employed. To obtain the zero-pressure bulk modulus, we vary the volume around the zero pressure volume V_0. We then use Murnaghans, Birchs, and Vinets equation of state (EOS)[57–59] as well as a spline fit for fitting the calculated E–V data. The E–V curves are transformed to enthalpy-pressure diagrams by extracting the pressure p through numerical differentiation of the equations of state ($p=-\partial E/\partial V$) and subsequently calculating the enthalpy H by using $H=E+pV$. Neglecting entropy effects due to the small difference in entropy between solid-state crystal structures and the comparably larger changes of ΔH within 1 GPa of pressure change, we chose the enthalpy difference ΔH as an appropriate measure to compare the relative stability of solid-state structures under pressure.

Acknowledgements

Financial support by the Deutsche Forschungsgemeinschaft, (priority program SPP 1236, project SCHN 377/13) as well as the Fonds der Chemischen Industrie (FCI), Germany, and the Dr. Klaus Römer foundation, Munich (grant for S.R.R.), is gratefully acknowledged. Furthermore we thank the Leibniz Rechenzentrum, Munich, for computational resources on the Linux Cluster System.

[1] Y. H. Jeong, J. H. Lee, Y. T. Hong, *Appl. Phys. Lett.* **1990**, *57*, 2680–2682.
[2] Y. H. Jeong, G. T. Kim, K. I. Kim, U. J. Jeong, *J. Appl. Phys.* **1991**, *69*, 6699–6700.
[3] Y. Hirota, T. Hisaki, O. Mikami, *Electron. Lett.* **1985**, *21*, 690–691.
[4] J. A. Graves, U.S. Patent 3475072, **1969**.
[5] M. S. Choudhary, J. K. Fink, K. Lederer, H. A. Krässig, *J. Appl. Polym. Sci.* **1987**, *34*, 863–869.
[6] R. Briegleb, H. Genther, *Liebigs Ann. Chem.* **1862**, *123*, 228–241.
[7] a) S. Horstmann, E. Irran, W. Schnick, *Angew. Chem.* **1997**, *109*, 1938–1940; *Angew. Chem. Int. Ed. Engl.* **1997**, *36*, 1873–1875; b) S. Horstmann, E. Irran, W. Schnick, *Z. Anorg. Allg. Chem.* **1998**, *624*, 620–628.
[8] K. Landskron, H. Huppertz, J. Senker, W. Schnick, *Angew. Chem.* **2001**, *113*, 2713–2716; *Angew. Chem. Int. Ed.* **2001**, *40*, 2643–2645.
[9] K. Landskron, H. Huppertz, J. Senker, W. Schnick, *Z. Anorg. Allg. Chem.* **2002**, *628*, 1465–1471.
[10] P. Kroll, W. Schnick, *Chem. Eur. J.* **2002**, *8*, 3530–3537.
[11] F. Karau, W. Schnick, *J. Solid State Chem.* **2005**, *178*, 135–141.
[12] F. Karau, W. Schnick, *Angew. Chem.* **2006**, *118*, 4617–4620; *Angew. Chem. Int. Ed.* **2006**, *45*, 4505–4508.
[13] K. Landskron, E. Irran, W. Schnick, *Chem. Eur. J.* **1999**, *5*, 2548–2553.
[14] F. W. Karau, L. Seyfarth, O. Oeckler, J. Senker, K. Landskron, W. Schnick, *Chem. Eur. J.* **2007**, *13*, 6841–6852.
[15] F. Karau, W. Schnick, *Z. Anorg. Allg. Chem.* **2006**, *632*, 231–237.
[16] F. Karau, Dissertation, Ludwig-Maximilians-Universität München (Germany), **2007**.
[17] A. Zerr, G. Miehe, G. Serghiou, M. Schwarz, E. Kroke, R. Riedel, H. Fueß, P. Kroll, R. Boehler, *Nature* **1999**, *400*, 340–342.
[18] M. Schwarz, G. Miehe, A. Zerr, E. Kroke, B. T. Poe, H. Fuess, R. Riedel, *Adv. Mater.* **2000**, *12*, 883–887.
[19] K. Komeya, M. Matsui in *Materials Science and Technology, Vol. 11* (Eds.: R. W. Cahn, P. Haasen, E. J. Kraemer), Wiley-VCH, Weinheim **1994**, pp. 518–565.
[20] *Chalcedon in Römpps Lexikon Chemie, Vol. 1*, 10th ed., (Eds.: J. Falbe, M. Regitz), Thieme, Stuttgart **1996**, p. 652; *Hardness of Materials and Minerals in Handbook of Chemistry and Physics*, 88th ed. (Ed.: D. R. Lide), CRC Press, Boca Raton, **2007**, pp. 12–216.
[21] TREOR90, P.-E. Werner, University of Stockholm, Stockholm, **1990**.
[22] P.-E. Werner, *Z. Kristallogr.* **1964**, *120*, 375–389.
[23] P.-E. Werner, L. Errikson, M. Westdahl, *J. Appl. Crystallogr.* **1985**, *18*, 367–370.
[24] STOE WinXPOW, v. 1.2, STOE & Cie GmbH, Darmstadt, **2001**.
[25] W. L. Bragg, *Proc. R. Soc. London Ser. A* **1927**, *113*, 642–657; P. Hartmann, *Z. Kristallogr.* **1989**, *187*, 139–143.
[26] The terms *dreier*, *vierer*, and *sechser* ring were coined by Liebau and are derived from the German words "drei" (three), "vier" (four) and "sechs" (six). However, for example a *dreier* ring is not a three-membered ring, but a six-membered ring comprising *three* tetrahedra centers (here P and Be) and *three* electronegative atoms (N). Similar terms exist for rings comprising different numbers of tetrahedra centers (and the corresponding number of electronegative atoms), respectively. F. Liebau, *Structural Chemistry of Silicates*, Springer, Berlin **1985**..
[27] P. Hartmann, *Z. Kristallogr.* **1989**, *187*, 139–143.
[28] D. Hardie, K. H. Jack, *Nature* **1957**, *180*, 332–333.
[29] O. Reckeweg, C. Lind, A. Simon, F. J. DiSalvo, *Z. Naturforsch. B* **2003**, *58*, 159–162.
[30] R. D. Shannon, *Acta Crystallogr. Sect. A* **1976**, *32*, 751–767.
[31] W. H. Baur, *Crystallogr. Rev.* **1987**, *1*, 59–83.

[32] U. Müller, *Anorganische Strukturchemie*, 3rd ed., Teubner, Stuttgart, **1996**.
[33] R. P. Ziebarth, J. D. Corbett, *J. Am. Chem. Soc.* **1988**, *110*, 1132–1139; R. P. Ziebarth, J. D. Corbett, *Inorg. Chem.* **1989**, *28*, 626–631; M. Köckerling, R. Y. Qi, J. D. Corbett, *Inorg. Chem.* **1996**, *35*, 1437–1443; R. Y. Qi, J. D. Corbett, *Inorg. Chem.* **1995**, *34*, 1646–1651; J. Zhang, J. D. Corbett, *Z. Anorg. Allg. Chem.* **1991**, *598/599*, 363–370.
[34] C.-M. Sung, M. Sung, *Mater. Chem. Phys.* **1996**, *43*, 1–18.
[35] F. Gao, R. Xu, K. Liu, *Phys. Rev. B* **2005**, *71*, 052103/1–4.
[36] R. Ahuja, L. S. Dubrovinsky, *J. Phys. Condens. Matter* **2002**, *14*, 10995–10999.
[37] A. Zerr, M. Kempf, M. Schwarz, E. Kroke, M. Göken, R. Riedel, *J. Am. Ceram. Soc.* **2002**, *85*, 86–90.
[38] J. Z. Jiang, H. Lindelov, L. Gerward, K. Stahl, J. M. Recio, P. Mori-Sanchez, S. Carlson, M. Mezouar, E. Dooryhee, A. Fitch, D. J. Frost, *Phys. Rev. B* **2002**, *65*, 161202/1–4.
[39] P. Kroll, M. Milko, *Z. Anorg. Allg. Chem.* **2003**, *629*, 1737–1750.
[40] W. Y. Ching, Y.-N. Xu, P. Rulis, *Appl. Phys. Lett.* **2002**, *80*, 2904–2906.
[41] K. Leinenweber, M. O'Keeffe, M. Somayazulu, H. Hubert, P. F. McMillan, G. H. Wolf, *Chem. Eur. J.* **1999**, *5*, 3076–3078.
[42] E. Soignard, D. Machon, P. F. McMillan, J. Dong, B. Xu, K. Leinenweber, *Chem. Mater.* **2005**, *17*, 5465–5472.
[43] G. Brauer, *Handbuch der Präparativen Anorganischen Chemie*, 3rd ed., Ferdinand Enke, Stuttgart, **1975**.
[44] J. Lücke, Dissertation, Rheinische Friedrich-Wilhelms-Universität Bonn (Germany), **1994**.
[45] V. van Kampen, T. Mensing, P. Welge, K. Straif, T. Brüning in *Toxikologisch-arbeitsmedizinische Begründungen von MAK-Werten* (Ed: H. Greim), Wiley-VCH, Weinheim, **2003**.
[46] GSAS, General Structure Analysis System, R. B. von Dreele, A. C. Larson, Los Alamos National Laboratory, Los Alamos, **2000**.
[47] P. Hohenberg, W. Kohn, *Phys. Rev. B* **1964**, *136*, 864–871.
[48] G. Kresse , J. Hafner, *Phys. Rev. B* **1993**, *47*, 558–561; G. Kresse, J. Hafner, *Phys. Rev. B* **1994**, *49*, 14251–14269.
[49] G. Kresse, J. Furthmüller, *Comput. Mater. Sci.* **1996**, *6*, 15–50.
[50] G. Kresse, J. Furthmüller, *Phys. Rev. B* **1996**, *54*, 11169–11186.
[51] J. P. Perdew, A. Zunger, *Phys. Rev. B* **1981**, *23*, 5048–5079.
[52] J. P. Perdew in *Electronic Structures of Solids '91*, (Eds.: P. Ziesche, H. Eschrig), Akademie Verlag, Berlin, **1991**.
[53] J. P. Perdew, J. A. Chevary, S. H. Vosko, K. A. Jackson, M. R. Pederson, D. J. Singh, C. Fiolhais, *Phys. Rev. B* **1992**, *46*, 6671–6687.
[54] P. E. Blöchl, *Phys. Rev. B* **1994**, *50*, 17953–17979.
[55] G. Kresse, J. Joubert, *Phys. Rev. B* **1999**, *59*, 1758–1775.
[56] H. J. Monkhorst, J. D. Pack, *Phys. Rev. B* **1976**, *13*, 5188–5192.
[57] F. D. Murnaghan, *Proc. Natl. Acad. Sci. U.S.A.* **1944**, *30*, 244–247.
[58] F. Birch, *J. Geophys. Res.* **1952**, *57*, 227–286.
[59] a) P. Vinet, J. R. Smith, J. Ferrante, J. H. Rose, *Phys. Rev. B* **1987**, *35*, 1945–1953; b) P. Vinet, J. H. Rose, J. Ferrante, J. R. Smith, *J. Phys. Condens. Matter* **1989**, *1*, 1941–1963.

Received: January 20, 2010
Published online: May 12, 2010

